Effect of welding speed on Nd:YAG laser weldability of ZE41A-T5 magnesium sand castings

H. Al-Kazzaz, M. Medraj
Mechanical and Industrial Engineering Department
Concordia University
1455 de Maisonneuve Boulevard West
Montreal, Quebec, Canada H3G 1M8

X. Cao, M. Jahazi, M. Xiao
Aerospace Manufacturing Technology Centre, Institute for Aerospace Research
National Research Council Canada
5145 Decelles Avenue
Montreal, Quebec, Canada H3T 2B2

ABSTRACT

The 2-mm butt joints of ZE41A-T5 sand castings were laser welded using 1.6 mm EZ33A-T5 filler wire and a continuous wave Nd:YAG system at a power of 4 kW, surface defocusing and various welding speeds. Compared with the base metal, the fusion zone showed significant grain refinement due to high cooling rate. No grain coarsening was observed in the heat affected zone (HAZ). The porosity area percentage and total solidification crack length in the fusion zone (FZ) were reduced as the welding speed increased from 4 to 7 m/min. Fusion zone area, total penetration depth, and weld width decreased with increased welding speed. The hardness in the FZ was similar to or higher than the base metal after a natural aging of about one year, but there was a drop in the hardness of the HAZ. The HAZ width decreased with increasing the welding speed. Tensile test showed that a joint efficiency of approximately 75 – 90 % was obtained.

MET SOC

Light Metals 2005
44th Annual Conference of Metallurgists of CIM
Calgary, Alberta, Canada
Edited by **J.-P. Martin**

INTRODUCTION

Magnesium alloys are becoming one of the most important alloys in the 21st century due to the low density and excellent specific strength, excellent damping capacities (good impact and noise reduction), good castability and machinability (1, 2). Therefore, they have found considerable applications in aerospace, aircraft and automotive industries. For instance, ZE41A-T5 (Mg-4.2Zn-1.2Ce-0.7Zr) sand cast Mg alloy has been used in aircraft engine casing, auxiliary gearbox, gearbox casing, etc (3). Nearly 85 – 90% of magnesium alloys are manufactured by casting processes, due to the limited workability as a consequence of the HCP crystal structure.

The increase in magnesium applications highlights the need to develop a proper joining technology. Today, tungsten inert gas (TIG) and metal inert gas (MIG) processes are the main welding methods for Mg alloys. In general magnesium alloys are difficult to weld due to the following reasons: oxidation, porosity and crack formation especially when Mg alloys contain more than 6% Al and 1% Zn (4, 5) or more than 3% Zn (3), large fusion zone (FZ) and heat-affected zone (HAZ) as a consequence of excessive heat input. These difficulties of Mg alloys can be overcome by applying high power density laser or electron beam welding processes. Since laser welding can be performed under ambient pressure, it is preferred over the electron beam technique. Therefore, high attention is directed towards laser welding for Mg alloys.

Laser welding process, has many advantages over the conventional welding processes. It has low heat input (6), high power density (6), high welding speed (2), narrow heat-affected zone (6), ease to automate (6), deep penetration depth (7) and thus high aspect ratio (depth/width), low distortion (8), in addition to the possibility of welding with and without filler wire. The use of filler wire in laser welding of Mg alloys still in its infant stage, but it is getting more attention since it might solve many problems related to the autogenous (without filler wire) welding such as: improvement in weld properties (8), welding of thick sections through multipass techniques (7) reduction in porosity (4) and crack.

The ongoing project is conducted to investigate the laser weldability of ZE41A-T5 with the objective to develop a reliable welding and repairing process. This paper reports on the effect of welding speed on the laser weldability of 2-mm ZE41A-T5 sand castings using 1.6 mm EZ33A-T5 filler wire.

EXPERIMENTAL PROCEDURES

The experimental material was sand cast ZE41A-T5 magnesium alloy used generally for engine casings. The cast plates had sizes of approximately 300 x 150 x 3-4 mm. Every casting was then cut into four small pieces for laser welding, each with

approximate sizes of 150 x 75 x 3-4 mm. The magnesium castings were machined to 2 mm thickness. The joint faces were also machined along the length for all the specimens. Prior to laser welding the joint faces and their surroundings were carefully cleaned by acetone to remove any contaminations.

The laser welding machine used was a continuous wave (CW) 4 kW HL4006 Nd:YAG (neodymium-doped yttrium aluminum garnet) laser system equipped with an ABB robotic and magnetic fixture system. A focal length of 150 mm and a fiber diameter of 0.6 mm were employed. Helium was used to shield the top and bottom surface of the workpieces. Its flow rates were 18.9 and 21.2 l/min (40 and 45 cubic feet per hour) for the top and bottom surfaces, respectively. The shielding gas was directed to the top surface of the workpiece at an angle of 30° and was vertically and uniformly directed to the bottom surface. The workpieces were positioned and clamped in a fixture and the butt joint with a gap of 0.4 mm was used. Zero defocusing (surface defocusing) with 0.45 mm focal spot diameter was used.

The filler metal EZ33A-T5 (1.6 x 990 mm for each wire) was used through a continuous feeding mechanism. The position of the filler wire was just above the surface of the workpiece. During laser welding, the workpieces were stationary while the laser beam scanned at a power of 4 kW and different speed (4, 5, 6, and 7 m/min). Wire feeding rate was calculated by using volume flow rate constancy equation (9):

$$\text{Wire feed rate} = \frac{\textit{welding speed x gap area}}{\textit{filler wire area}} \quad (1)$$

The laser weldability of sand cast ZE41A-T5 magnesium alloy was examined through microstructure and mechanical tests. A length of approximately 20 mm was cut from both ends of each joint to exclude the unstable segments at the start and end of laser welding. Cross-sectional samples for metallurgical examination were cut from the weld joints at three locations (start, middle and end). These cut specimens were mounted using hot-setting resin and polished to a mirror-like finish. The polished samples were then etched in Nital solution. The microstructure details were examined using Olympus optical microscope equipped with Discover Essential image analyzer software. The average values were calculated from the quantitive measurements of the three specimens (start, middle and end). The middle specimen was also used for the Vickers microindentation hardness test by using Duramin A-300 hardness Tester, under a test force of 200 g and dwell period of 15 seconds. Four tensile-specimens cut from each weld joint were prepared according to ASTM standards (B557M-02A). The samples were examined for the tensile test at constant strain rate (0.01 mm/sec) by using MTS-100 KN tensile test machine.

RESULTS AND DISCUSSION

Weld Geometry

To analyze the weld geometry of the tested samples, the average weld width (average of top and root bead width), penetration depth, crown height, root height, crown area, root area, and total weld area were measured. The effect of welding speed on the width, height and weld area are shown in Figures 1 and 2. As expected, the weld dimensions decreased with increased welding speed. As the welding speed increases the laser fluence (eq-2) decreases implying that less heat was absorbed by the workpiece resulting in smaller melted weld area and joint size.

$$Laser\ Fluence = \frac{Laser Power}{Focal Spot Diam\ x\ Welding Speed} \quad (2)$$

The sample tested at 7 m/min shows slight deviations due to the large misalignment of the work-pieces. At high welding speed, it was found that the 1.6 mm filler wire was difficult to melt due to the small diameter of beam laser. The aspect ratios for all sections were greater than 1.2 indicating that the keyholes were established during the welding (3).

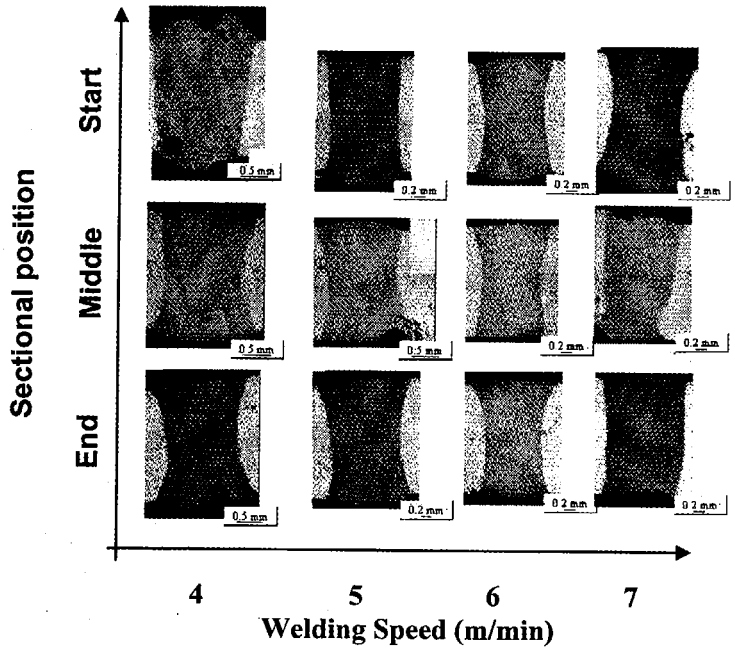

Figure 1 – Effect of Welding Speed on Weld Geometry

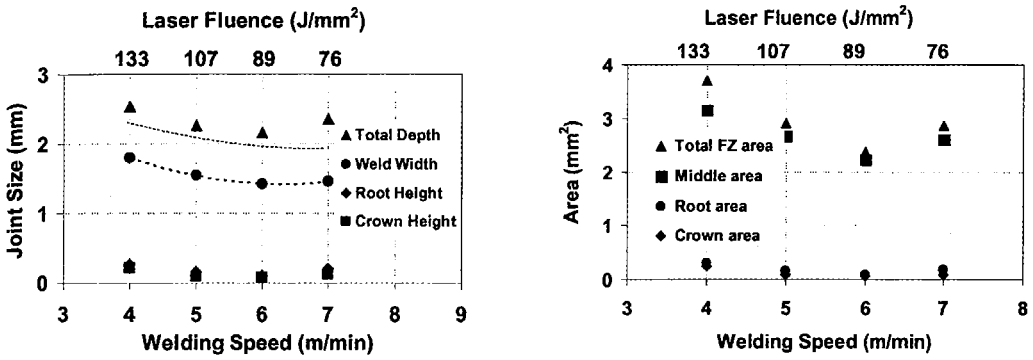

a) b)

Effect of Welding Speed on (a) Joint Size and (b) Weld Area

Higher crown and root heights were observed in the sample welded at 4 m/min (starting section as shown in Figure 1). The excessive crown and root heights might increase the stress concentration in these areas (10). The large crown obtained in this sample is probably due to the expansion and flotation of the pores (5). As well known, the use of filler wire might reduce the tendency to form underfill. The sample welded at 5 m/min (middle section as shown in Figure 1) showed a root underfill near the base metal (BM), probably due to BM defect. The sample welded at 7 m/min (ending section as shown in Figure 1) showed shrinkage groove at the root. The sample welded at 6 m/min showed smooth top and root bead surface with narrow and uniform weld width, which was the optimum weld geometry obtained among the tested samples.

Microstructure

Figure 3 shows that laser welding also produces three distinct regions: fusion zone (FZ), partially melted zone (PMZ) and heat-affected zone (HAZ). It was observed that the grains in the FZ was significantly finer than those in the BM and HAZ, which can be attributed to the high cooling rate (10^5 – 10^6 °C/s) obtained in laser welding process compared with the low cooling rate (10^2 – 10^3 °C/s) obtained in arc welding (11).

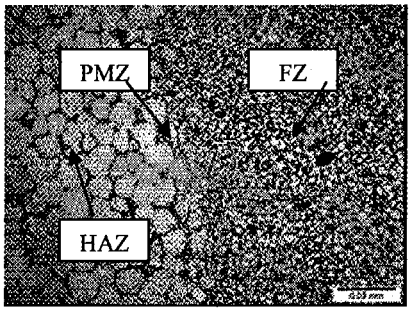

Figure 2 – Micrograph Showing the FZ, PMZ and HAZ

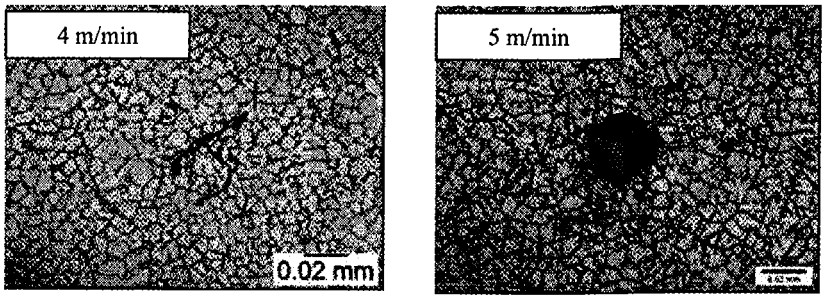

Figure 4 – Micrographs Showing the Grain Morphology in the FZ

The fusion zone microstructure was observed to be fine equiaxed or rosette grains as shown in Figure 4. Although the welding speed increased from 4 to 7 m/min, no significant change in grain size in the FZ was observed. The fine equiaxed grains obtained in laser process can also be attributed to Zr in the ZE41A-T5 alloy. It was reported that grain refining of magnesium alloys seems to be based on a peritectic reaction on Zr nuclei (11). Originally, the grains nucleate as small spheres around the initiating Zr particles. Because the nucleation is so prolific, many grains are nucleated at once and the grains cannot grow far before they mutually impinge. Figure 3 shows that the partial melting zone (PMZ) is rather narrow, only one or two grains wide. This figure also shows the cellular growth from the large grains in the PMZ. The length of the cellular growth is approximately similar to the grain size in the FZ. This limited cellular growth can be attributed to the high cooling rate and the presence of prolific Zr nuclei. It was difficult to distinguish the difference in microstructure between the HAZ and base metal. Therefore, no grain coarsening was observed in the HAZ. For this reason the HAZ was identified by the microindentation hardness as discussed later.

Porosity

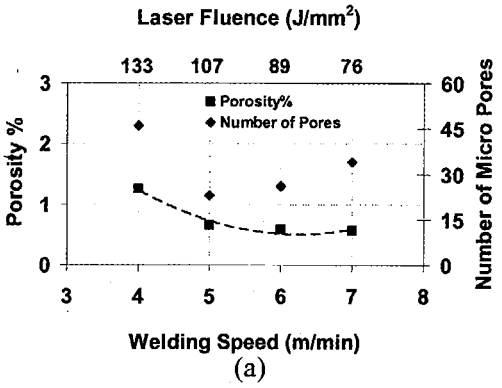

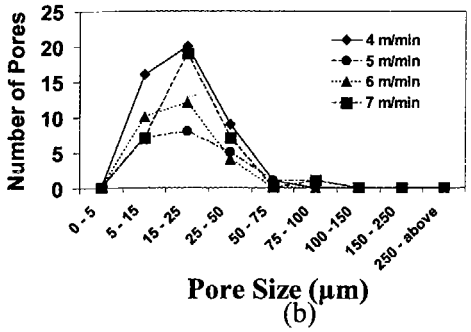

Figure 5 – (a) Effect of Welding Speed on Porosity (b) Porosity Distribution

The relation of porosity area percentage and number with welding speed is shown in Figure 5 (a). The porosity area percentage decreased from 1.26% to 0.57% as the welding speed increased from 4 to 7 m/min. Although it was difficult to find the trend between the welding speed and number of pores, in general increasing the welding speed reduces the number of pores. Figure 5 (b) shows the average pores size distribution for all samples. It was observed that the majority of pores were smaller than 75 μm, with typical size about 20 μm.

Keyhole instability is considered to be one of the most important reasons for porosity formation in Al alloys. The stability of the keyhole depends on the balance between the vapor pressure and the surface tension (12). The vapor pressure tends to open the keyhole whereas the surface tension tends to close it. The collapse of the keyhole takes place when there is a sudden drop in vapor pressure causing the molten metal to slump into the keyhole. Compared with Al-alloys, Mg alloys have low surface tension and high vapor pressure (due to evaporative elements such as Zn, Mg, etc.) leading to the formation of a more stable keyhole (13).

In addition, Mikucki et al. (14) reported that the porosity in AZ91 Mg alloy was dependent on the amount of dissolved hydrogen in the alloy. The rejection of hydrogen from the solid-liquid interface assisted in the nucleation and growth of micro porosity during solidification. Regarding ZE41A-T5 Mg alloy (which contains Zr element) hydrogen will react with zirconium to form ZrH_2. Hence, hydrogen should not be the main source for the formation of porosity in the experimental alloy ZE41A-T5 (11).

Zhao et al. (5, 13), Haferkamp et al. (4) and Lenhner et al. (15) reported that the coalescence and expansion of preexisting pores in the base metal (BM) is responsible for the porosity formation. The applied heat by the laser beam may increase the pressure inside the pores causing the expansion and coalescence to form bigger pores practically at lower welding speed as shown in Figure 1. The maximum porosity percentage measured was 1.26% at 4 m/min but it is considered to be low compared with the published data for other Mg alloys (5). The main reason may be due to the use of filler wire, which has low preexisting pores since it was produced by extrusion process.

Crack

Weld cracks were observed for ZE41A-T5 alloy. For all tested samples the area of solidification cracks was less than 1 mm^2 thus these cracks are micro-cracks (16). The maximum total crack length in the fusion zone was 1.47 mm, and the maximum average width was 2 μm for the sample welded at 4 m/min. It was observed that increasing the welding speed from 4 to 7 m/min reduced the total crack length from 1.47 to 0.68 mm and reduced number of cracks from 9 to 5, as shown in Figure 6. The higher welding speed reduces solidification cracks, which seems to agree with the published results of AZ31 Mg alloy (17). Increasing the welding speed will reduce laser heat input, which may cause simultaneous solidification of the low melting phases with alloy matrix phase. The low crack formation experienced here may attributed to the followings: (i) formation

of fine microstructure in the FZ (which reduces the susceptibility for cracking), (ii) using the filler wire EZ33A-T5, since the filler wire helps to reduce evaporative losses of alloying elements and reduce the porosity formation, and (iii) rare earths elements in the experimental alloy and the filler wire, which beneficially narrow the freezing range and thus reduce the tendency of crack formation.

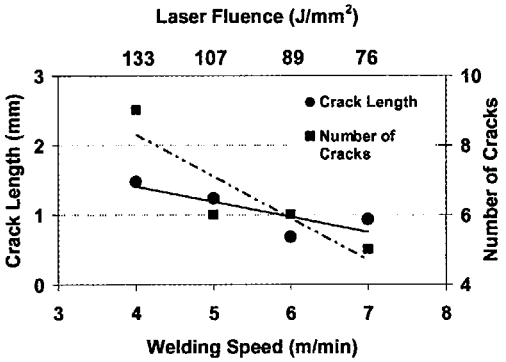

Figure 6 – Effect of Welding Speed on Crack Length and Number of Solidification Cracks in the FZ

Solidification crack occurs in the liquid films which surround the solidifying grains. These films have low melting temperature and appear to be brittle (9), causing cracking when subjected to high transverse contracting stresses induced during the rapid solidification process (Figure 7a). According to Borland's theory (18, 19), alloying elements with high solubility and low partitioning coefficients (e.g. Zn in Mg alloys) can increase solidification cracking susceptibility by promoting large freezing temperature range (20). The ZE41A-T5 alloy has wide solidification temperature range (120°C) (11). Thus, the occurrence of solidification crack is possible during the laser welding. Weld cracks may start from the area of high tensile stresses or stress raisers. Therefore, the cracks may initiate from oxide film, gas pores, shrinkage porosity and defects from the base metal (Figure 7).

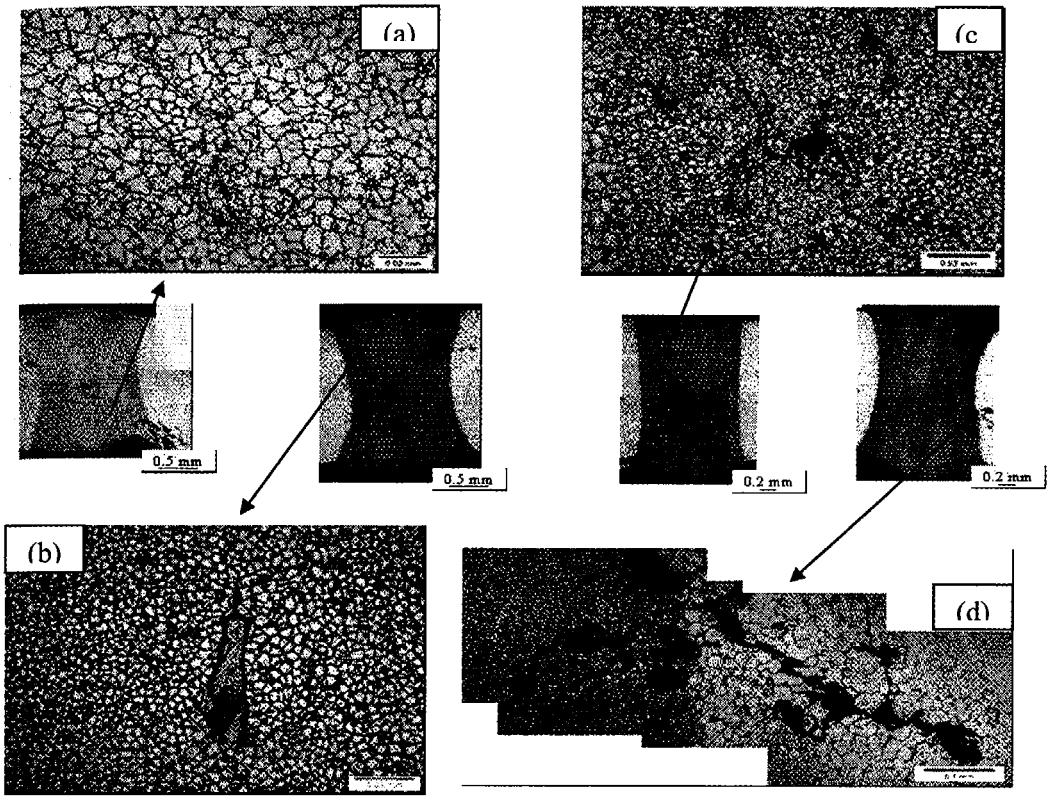

Figure 7 – Solidification Cracks in the FZ initiated by Various Sources Observed in Laser Welding of ZE41A-T5 Mg alloy

The liquation cracks were observed in the HAZ due to the liquation of some low melting intermetallics in the grain boundaries. Figure 8 shows a HAZ liquation crack obtained at welding speed of 5 m/min.

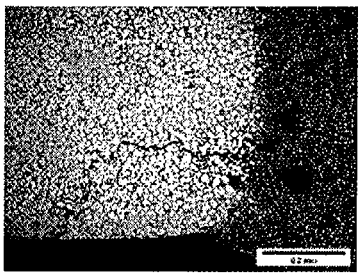

Figure 8 – HAZ Liquation Cracks Observed in Laser Welding of ZE41A-T5 Mg alloy

Micro-Indentation Hardness

Vickers microindentation hardness was measured over the weld joints as shown in Figure 9. These samples have had a natural aging over a period of approximately 12 months after the welding. The hardness values in the fusion zone have recovered to or even been higher than those in the base metal, probably due to the grain refinement in the FZ. However, there was a drop in the hardness in the heat affected zone. The width of the heat affected zone as indicated in Figure 10 varies from 2.5 to 1 mm as the welding speed increased from 4 – 7 m/min. As the welding speed increased the total heat input decreased and thus the heat transferred from FZ to the base metal was reduced resulting in smaller HAZ. The softening of the HAZ in the precipitate-hardenable alloys probably involves the dissolution of the strengthening phase Mg_9Ce and the formation and growth of nonstrengthening phases (11). The scattered data of the hardness in the base metal are probably due to low load used in the test (200 g), cast micro-defects, and non-uniform cooling rate during casting.

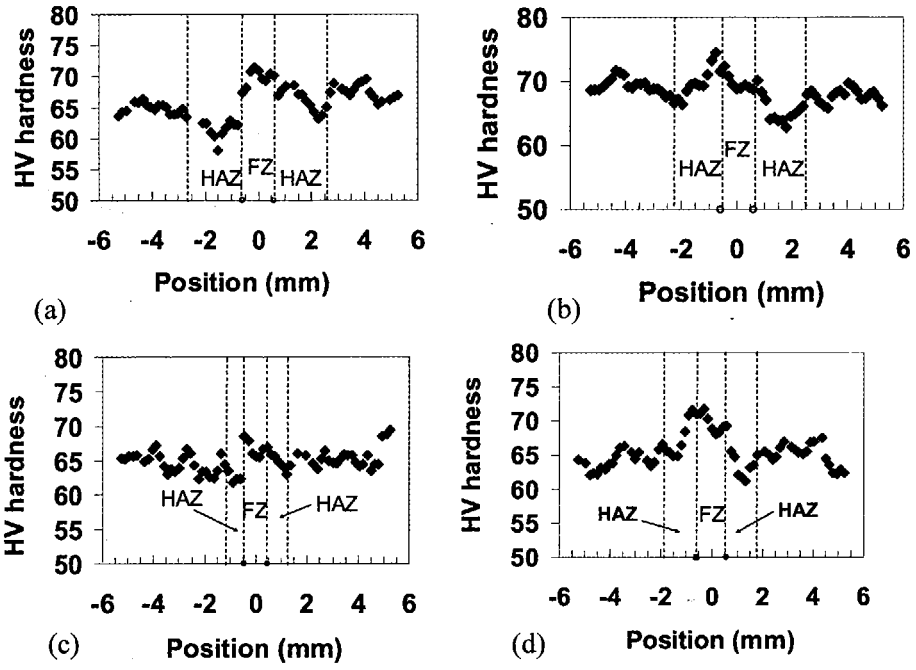

Figure 9 – Vickers Microindentation Hardness for Welding Speed at (a) 4, (b) 5, (c) 6, and (d) 7 m/min

Tensile Strength

Four tensile specimens were prepared from each joint except the one welded at 7 m/min because of the large misalignment. The joint efficiency of the test samples are shown in Figure 10. The joint efficiency is defined as the percent ratio of the ultimate

tensile strength of the weld joint to that of the base metal (here 179 MPa according to AMS-4439). It is found that the weld joints have a joint efficiency of approximately 75-90%. Only two specimens out of 12 failed in the FZ, whereas all the other fractured in the base metal at a distance of 4 to 22 mm from the PMZ. Most of the samples fractured in the base metal indicating that the FZ is stronger than the BM. One of the samples failed in the FZ shows low tensile property due to a visible big defect in the FZ.

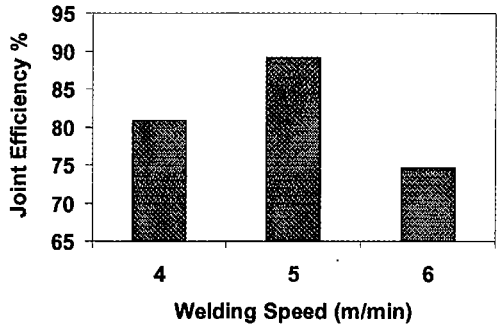

Figure 10 – Joint Efficiency of Laser Welded ZE41A-T5 Mg Alloy Using Filler Wire

CONCLUSIONS

A continuous wave Nd:YAG laser system was used to weld 2–mm butt joints of ZE41A-T5 sand castings using EZ33A-T5 filler wire at a power of 4 kW, surface defocusing, and variable speeds (4 – 7 m/min). The following conclusions can be drawn:

1 The penetration depth, average weld width and weld area decreased with increasing the welding speed.
2 A significant grain refinement is observed in the FZ due to high cooling rate. No grain coarsening occurs in the HAZ.
3 Increasing welding speed reduces porosity area percentage. Majority of the pores were observed to be smaller than 75 μm, with typical pore size of 15 – 25 μm. The length and number of solidification cracks decreased with increasing the welding speed.
4 The microindentation hardness in the FZ is similar to or even higher than that of the BM after aging of approximately one year. The hardness dropped within the HAZ. The tensile test showed that a joint efficiency of 75 – 90 % was obtained. Most of the tensile samples were found to fracture in the base metal.

ACKNOWLEDGEMENTS

The authors are indebted to the Natural Sciences and Engineering Research Council of Canada (NSERC) and Fonds Québécois de la recherche sur la nature et les technologies (FQRNT) for their financial support.

REFERENCES

1. M. Dhahri, J. Masse, J. Mathieu, G. Barreau, and M. Autric, "Laser welding of AZ91 and WE43 Magnesium alloys for Automotive and Aerospace Industries," Advanced Engineering Materials, Vol. 3, No. 7, 2001, 504 – 507.

2. K. G. Watkins "Laser Welding of Magnesium Alloys," Magnesium Technology 2003, Proceedings of the Symposium held during the 2003 TMS Annual Meeting. Publisher: Minerals, Metals & Materials Society, San Diego, CA, United States, 2003, 153-156.

3. X. Cao, M. Xiao, M. Jahazi, and Y. L. Lin, "Continuous Wave Nd: YAG Laser Welding of Sand-Cast ZE41A-T5 Magnesium Sand Casting: Conduction or Key-hole Mode," Proceedings of the International Symposium on Aerospace Materials and Manufacturing: Development, Testing and Life Cycle Issues--Honoring William Wallace, 2nd, Aerospace Materials and Manufacturing: Development, Testing and Life Cycle Issues--Honoring William Wallace Hamilton, ON, Canada, 2004, 187-197.

4. H. Haferkamp, F. von Alvensleben , I. Burmester, and M. Niemeyer, "The Characteristics of Laser Beam Welded Magnesium Alloys," Proceeding of the Laser Material Processing Conference, ICALEO, Part 2, Laser Zentrum Hannover e.V., Hannover, Germany, 1997 G140-149.

5. M. Pastor, H. Zhao, and T. Debroy, "Continuous wave – Nd: yttrium – aluminum – garnet laser welding of AM60B magnesium alloy," Journal of Laser Applications, Vol. 12, No. 3, 2000, 91 – 100.

6. A. Weisheit, R. Galun, and B. L. Mordike, "CO_2 Laser Beam Welding of magnesium – Based Alloys," Welding Research (Miami), Vol. 77, No. 4, 1998, 149s – 154s.

7. Z. Sun and M. Kuo, "Bridging the joint with wire feed laser welding," Materials Processing Technology, Vol. 87, 1999, 213 – 222.

8. H. Haferkamp, M. Goede, A. Bormann, and P. Cordini, "Laser Beam Welding of Magnesium Alloys-New Possibilities Using Filler Wire and Arc Welding," Proceeding of the LANE: Laser Assisted Net Shape Engineering 3, 2001, 333-338.

9. C. Dawes, Laser Welding, McGraw-Hill, Inc., New York, NY, USA, 1992.

10. American Welding Society, American National Standard, B1.11, 2000.

11. X. Cao, M. Xiao, M. Jahazi, and J.-P. Immarigeon, "Continuous Wave Nd: YAG Laser Welding of Sand-Cast ZE41A-T5 Magnesium Alloys," Material Manufacturing Processes (Accepted in 2004).

12. W. W. Duley, Laser Welding, John Wiley & Sons., Toronto, 1999.

13. H. Zhao and T. Debroy, "Pore Formation during laser beam welding of Die – cast Magnesium alloy AM60B – Mechanism and Remedy," Welding Research (Miami, FL, United States), Vol. 80, No. 8, 2001, 204s-210s.

14. B. A. Mickucki and J. D. Shearhouse, Proceeding of Magnesium and Magnesium Properties and Applications for Automobiles Conference, Society of Automotive Engineers, Inc., Detroit, 1993, 107 – 115.

15. Lehner, G. Reinhart, and L. Schaller, "Welding of Die Casted Magnesium Alloys on Production Machines," Pt. 2, Proceedings of the Laser Materials Processing Conference, ICALEO'98, Laser Institute of America, 1998, F18-F27.

16. European Standard: Welding – Electron and Laser Beam Welded Joints – Guided on Quality Levels for Imperfections – Part 2, "Aluminum and Its Weldable Alloys," EN ISO 13919 – 2:2001, 2001.

17. Z. Sun, D. Pan, and J. Wei, "Comparative Evaluation of Tungsten Inert Gas and Laser Welding of AZ31 Magnesium Alloy." Science and Technology of Welding and Joining, Vol. 7, No. 6, 2002 , 343 – 351.

18. J.C. Borland, Generalized Theory of Super-Solidus Cracking in Welds (and Castings), Brit. Welding Research Assocn, 1960, Vol. 7, No. 8, 508 – 512.

19. J.C. Borland, Suggested Explanation of Hot Cracking in Mild and Low Alloy Steel Welds, Brit. Welding Research Assocn., 1960, Vol. 8, No. 11, 526 – 540 (1960b).

20. M. Marya, G. Edwards, S. Marya, and D.L. Olson, "Fundamental in the Fusion Welding of Magnesium and Its Alloys," Proc. 7th JWS Int. Symp., Kobe, 2001, 597-602.